Journal of Medicinal Chemistry

Article

pubs.acs.org/jmc

Structure-Based Discovery of Substituted 4,5′-Bithiazoles as Novel DNA Gyrase Inhibitors

Matjaž Brvar,[†] Andrej Perdih,*[,†] Miha Renko,[‡,§] Gregor Anderluh,[∥,⊥] Dušan Turk,[‡,§] and Tom Solmajer*[,†]

[†]National Institute of Chemistry, Laboratory for Biocomputing and Bioinformatics, 1001 Ljubljana, Slovenia

[‡]Jozef Stefan Institute, Department of Biochemistry and Molecular Biology, 1000 Ljubljana, Slovenia

[§]Center of Excellence for Chemistry and Biology of Proteins, Jamova 39, 1000 Ljubljana

[∥]Biotechnical Faculty, Infrastructural Center for Surface Plasmon resonance, 1000 Ljubljana, Slovenia

[⊥]National Institute of Chemistry, Laboratory for Biosynthesis and Biotransformation, 1001 Ljubljana, Slovenia

Supporting Information

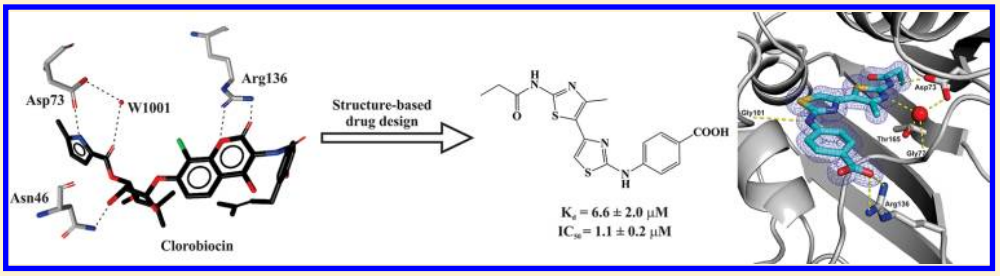

ABSTRACT: Bacterial DNA gyrase is a well-established and validated target for the development of novel antibacterials. Starting from the available structural information about the binding of the natural product inhibitor, clorobiocin, we identified a novel series of 4′-methyl-N^2-phenyl-[4,5′-bithiazole]-2,2′-diamine inhibitors of gyrase B with a low micromolar inhibitory activity by implementing a two-step structure-based design procedure. This novel class of DNA gyrase inhibitors was extensively investigated by various techniques (differential scanning fluorimetry, surface plasmon resonance, and microscale thermophoresis). The binding mode of the potent inhibitor **18** was revealed by X-ray crystallography, confirming our initial in silico binding model. Furthermore, the high resolution of the complex structure allowed for the placement of the Gly97−Ser108 flexible loop, thus revealing its role in binding of this class of compounds. The crystal structure of the complex protein G24 and inhibitor **18** provides valuable information for further optimization of this novel class of DNA gyrase B inhibitors.

1. INTRODUCTION

The wide utilization of antibiotics in previous decades has resulted in the increased incidence of bacterial resistance to most of the available antibacterials, resulting in the urgent need for novel and more efficient agents in this field.[1] Current research continues to discover new potential targets and novel compounds with broad spectra of efficacy simultaneously by taking into account some additional important issues such as toxicity and ADME properties.[2,3]

At present, bacterial DNA gyrase, a type II topoisomerase from the GHKL (gyrase, HSP 90, histidine kinase, MutL) enzyme family, remains one of the most investigated and validated targets for the development of novel antibacterials. Its absence in the mammalian organism and the crucial role it plays in the bacterial DNA replication cycle make this enzyme a very suitable target for the development of potential drugs from the perspective of selective toxicity.[4,5] The main role of this enzyme is the introduction of negative supercoils into the circular bacterial DNA molecule changing the linking number by two in each enzymatic step with concurrent occurring ATP hydrolysis. DNA gyrase is a heterodimeric enzyme with an A2B2 structure. The role of the A subunit is the breakage and reunion of the double DNA strand, while the B subunit (DNA gyrase B) possesses the ATPase activity, providing a sufficient amount of energy for the DNA supercoiling.[6]

Currently, the 6-fluoroquinolone chemical class of molecules are the only DNA gyrase inhibitors used in clinical practice.[7] They act by binding to the complex formed between the DNA molecule and the DNA GyrA subunit, consequently stabilizing the complex, thus preventing the reunion of both DNA strands and ultimately stopping the bacterial replication cycle. They are mainly utilized in the treatment of respiratory and urinary infections; however, the occurrence of some serious side effects calls for novel research in this field.[8]

The ATP binding site is located on the DNA gyrase B subunit and was broadly studied for its potential inhibition because of its functional importance.[9] The research in this field dates back to the 1950s with the discovery of natural product ATPase coumarin inhibitors (Figure 1) from the *Streptomyces*

Received: March 21, 2012
Published: June 25, 2012

dx.doi.org/10.1021/jm300395d | *J. Med. Chem.* 2012, 55, 6413−6426

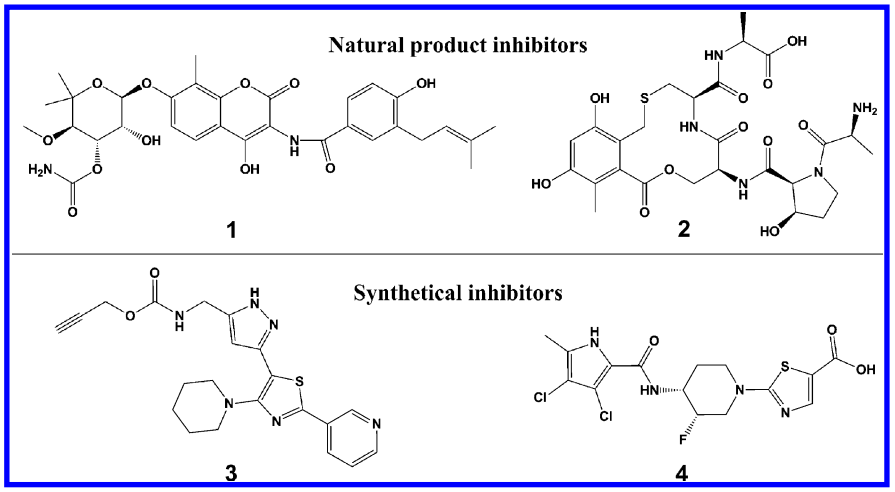

Figure 1. Chemical structures of natural product inhibitors of the DNA gyrase B **1** and cyclothialidine GR122222X (**2**) and two synthetic inhibitors from the chemical classes of pyrazolthiazoles (**3**)[14] and pyrrolamides (**4**).[15]

fungi species.[10] All coumarins are comprised of three moieties: the L-noviose sugar with the attached hydrogen bond donor group (5-methylpyrrole-2-carboxylic acid or carbamoyl group), the 3-aminocoumarin ring, and the 4-hydroxy-3-isoprenylbenzoyl moiety (Figure 1). Novobiocin (NVB, **1**) was licensed for clinical use in the 1960s but was quickly withdrawn from the market due to the occurrence of some serious toxicity issues.[11] The other two structurally similar coumarins, e.g., clorobiocin (CBN, **5**) and coumermycin, were also well described and characterized.[12,13]

Both **1** and **5** possess comparable inhibitory activities and similar binding modes, as revealed by the X-ray crystallography.[12,13,16−20] They both bind to the ATP-binding site, and the most important interactions of **5** in the *Escherichia coli* DNA gyrase ATP active site (PDB: 1KZN) are schematically presented in Figure 2. The hydrogen bond donating group attached to the sugar moiety interacts with Asp73 residue and via the conserved W1001 water molecule with Thr165 residue. The 5-methylpyrrole ring of **5** forms additional hydrophobic interactions with the residues Val43, Ala47, Val71, Ile78, Val120, and Val167, creating the hydrophobic pocket within the ATP binding site.[13] The hydroxyl group of the L-noviose sugar forms a hydrogen bond with the Asn46 residue, and both methyl groups contribute substantially to the hydrophobic interactions with the Ile 78 and Ile90. Two oxygen atoms of the coumarin ring form strong hydrogen bonds with the Arg136 residue and create one of the most important interactions responsible for tight ligand binding (Figure 2).[12,13,16] The importance of this interaction was further substantiated by mutations of R136H, which led to a significant loss of coumarin antibacterial activity.[21] The binding ratio for both **1** and **5** was determined to be 1:1, whereas one molecule of coumermycin binds to two GyrB subunits simultaneously.

To retain biological activity and improve the ADME properties of this chemical class of molecules that act only if applied intravenously, several attempts to optimize the coumarin class have been made by introducing different substitutions on the coumarin ring, preferably at the position 4,[22] making changes to the sugar part (L-noviose to L-rhamnose or cyclohexyl moiety)[23,24] or hydrogen bond donating group (*N*-propargyloxycarbamate). Recently, researchers at AstraZeneca developed a series of gyrase inhibitors starting from the pyrrole-2-carboxylic acid (Figure 1, compound **4**).[15] Some of

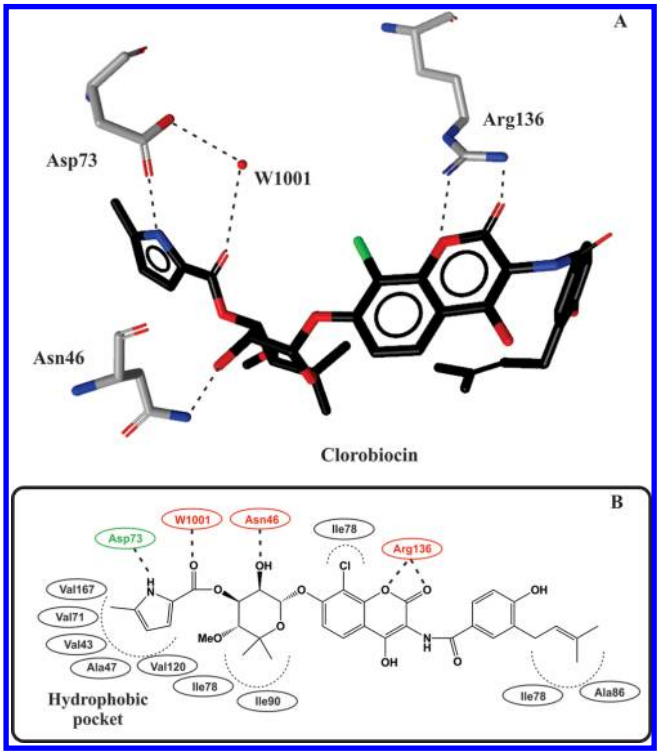

Figure 2. (A) Interaction binding pattern between **5** and *E. coli* DNA gyrase B ATP-binding site, as revealed by X-ray crystallography (PDB: 1KZN). Dotted lines represent hydrogen bonds between the inhibitor and the protein active site residues. (B) Green residue represents hydrogen bond acceptor, red residues hydrogen bond donors, and black residues form hydrophobic interactions.[13]

these changes resulted in potent compounds with favorable pharmacokinetic properties and are currently undergoing clinical trials; however, at present, no molecules have reached the market yet.[15]

The second class of the natural product inhibitors act by binding to the ATP-binding site of the bacterial DNA gyrase are cyclothialidines (Figure 1, compound **2**) from the same fungi species. They all include a substituted resorcinol ring with the attached pentapeptide chain (Cys, Ala, Ser, Pro, and Ala).[25−27] Despite their higher potency and better selectivity against eukaryotic topoisomerases in comparison to the

dx.doi.org/10.1021/jm300395d | J. Med. Chem. 2012, 55, 6413−6426

Scheme 1. Outline of the Computational and Experimental Work Presented in This Study[a]

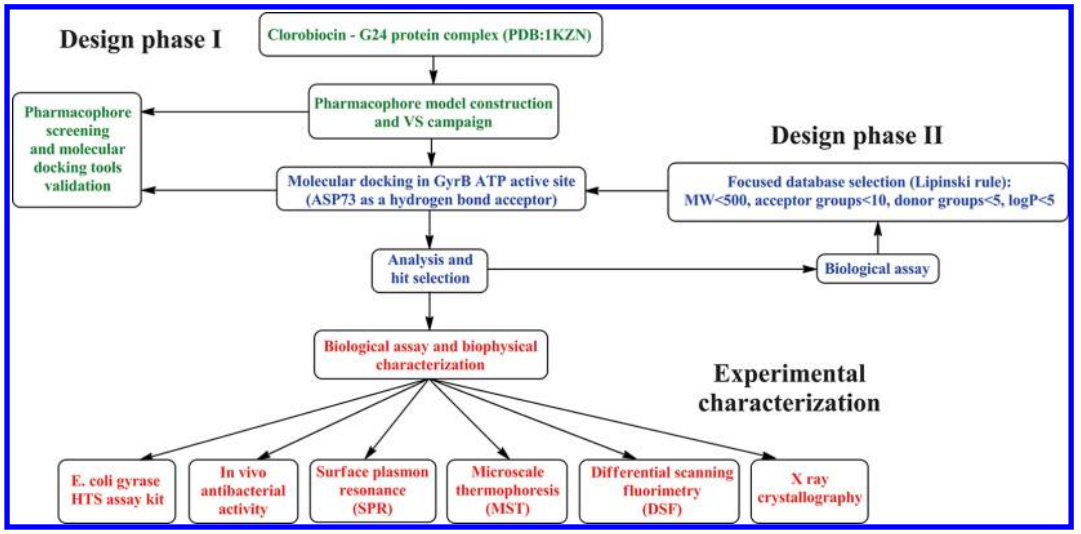

[a]The first phase of the design is presented in green, the second phase in blue, and the subsequent biophysical characterization in red. Molecular docking, analysis and hit selection were performed in both design steps.

coumarin class, they lack in vivo antibacterial activity due to their high lipophilicity. Recently, several fruitful attempts have been made to improve their water solubility and permeability characteristics and to increase their in vivo activity.[28−30]

Furthermore, compounds isolated from the *Camellia sinensis* plant, mainly epigallocatechin gallate, have also been shown to possess promising antigyrase activity, and their binding properties have been characterized using fluorescence spectroscopy and two-dimensional NMR spectroscopy.[31] In addition, a series of diacylglycoside quercetin derivatives has been developed which have also shown promising inhibitory activity against resistant bacterial strains such as vancomycin-resistant *Enterococcus* (VRE).[32] Following the structure−activity pattern of natural product compounds, other structural classes of low molecular weight inhibitors have been synthesized in the previous two decades. They are all composed of the same structural element: a hydrogen bond donor−acceptor pattern, which has been identified with the X-ray analysis as the crucial structural element for the inhibition of the DNA gyrase B. Synthetic inhibitors belong to the chemical classes of pyrrazoles (Figure 1, compound **3**),[14,33] triazines,[34] indolinones,[35,36] indazoles,[37] pyrimidines,[34] benzimidazole ureas,[38−40] and Schiff bases of indolinone-2,3-diones.[41] Taking the structural information about natural cyclothialidines into account, several phenol[42,43] and resorcinol[44] compounds were discovered as DNA gyrase B inhibitors. Many of these inhibitors possess even higher activity than their starting points from the pool of natural compounds; however, none of them have progressed to the clinic yet.

In the past, we have focused our research efforts on the development of the DNA gyrase B inhibitors starting from the cyclothialidine chemical class of natural gyrase inhibitors and identified several novel low molecular weight inhibitors from the resorcinol and phenol chemical classes.[43,44] In this study, we have focused our attention on the class of coumarin-based natural DNA gyrase B inhibitors as our starting point. The working outline of our multistep procedure is depicted in Scheme 1, showing a plethora of in silico and experimental methods used in our work. The two-step design process begins with the analysis of the crucial interactions between the **5**, a potent coumarin inhibitor of gyrase B, and the G24 protein, the smallest fragment of the N terminal part of the B subunit still able to bind the ATP molecule (PDB code: 1KZN).[13] Subsequently, a structure-based pharmacophore model was constructed and validated for further utilization in a large scale virtual screening (VS) campaign. Hit molecules from this first step of the VS procedure were additionally docked into the DNA gyrase B active site, and their predicted binding modes were visually inspected (Design phase I, Scheme 1, green). Selected commercially available compounds from different chemical classes were experimentally assayed for their gyrase inhibitory activity; a structural class of 4′-methyl-[4,5′-bithiazole]-2,2′-diamines was identified as a starting point for the second design phase (design phase II, Scheme 1, blue). In the search for even more potent compounds, we have constructed a focused library of this structural class, which was utilized in the molecular docking studies into the G24 ATP binding site to select a subset of novel promising molecules. Assayed compounds enabled the initial SAR information about the binding of this series. Furthermore, the most potent active compounds were characterized using a wide range of experimental techniques (experimental characterization, Scheme 1, red) such as surface plasmon resonance (SPR), microscale thermophoresis (MST), and differential scanning fluorimetry (DSF). The in vitro antibacterial activity against three different bacterial strains was determined, and finally two most potent compounds were used in the crystallography X-ray experiments to determine the binding mode of the most active compounds predicted and additionally enable the retrospective analysis of our in silico design steps and derived models.

2. RESULTS AND DISCUSSION

2.1. Design Phase I: The Structure-Based Virtual Screening Campaign and Biological Evaluation of the Selected Hit Compounds Starting from Clorobiocin Binding Structural Information. In our effort to identify novel potent gyrase inhibitors with drug-like properties, our design starting point was the structural information embodied in the crystal structure of the G24 protein, 24 kDa large N-terminal part of the B subunit of DNA gyrase, cocrystallized

dx.doi.org/10.1021/jm300395d | J. Med. Chem. 2012, 55, 6413−6426

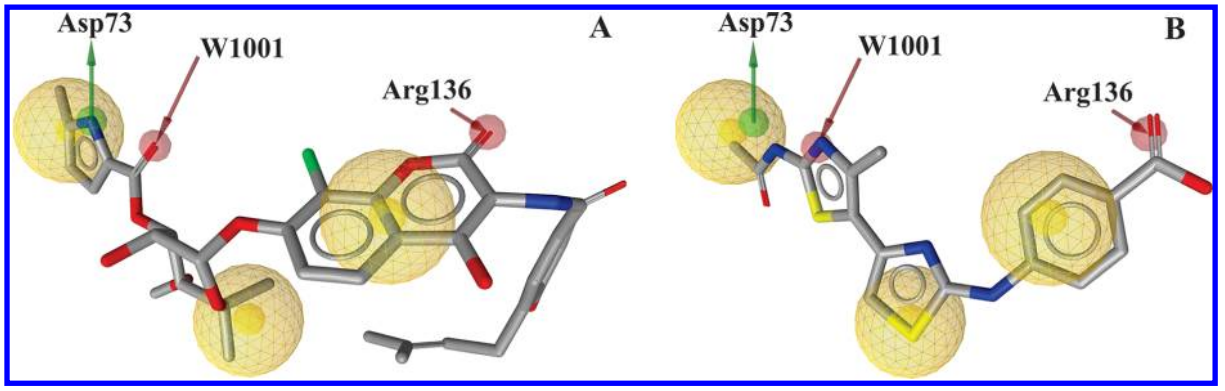

Figure 3. (A) Reduced structure-based pharmacophore model, created by using LigandScout software, describing the crucial interactions between molecule **5** and the G24 protein (PDB: 1KZN). Green arrows represent hydrogen bond donors, red arrows hydrogen bond acceptors, and yellow spheres hydrophobic areas. (B) Example of the LigandScout-generated conformation of the virtual hit **6** aligned to the pharmacophore model.

Table 1. Results of the Biological Assay of Selected Compounds 6−17 with Inhibitory Activity against the DNA Gyrase from Design Phase I

Compd	chemical structure	IC_{50} [μM]	Compd	chemical structure	IC_{50} [μM]
6	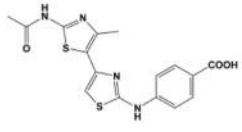	5	**12**	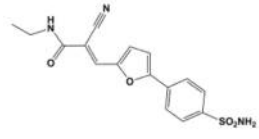	>1000
7	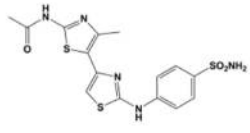	700	**13**	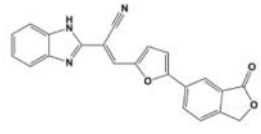	>1000
8	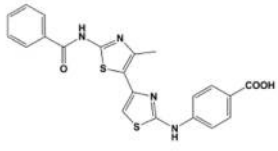	>1000	**14**	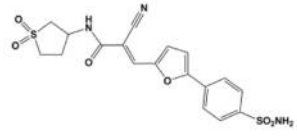	>1000
9	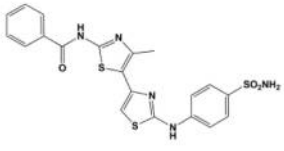	>1000	**15**	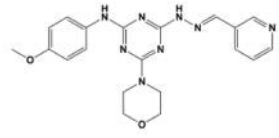	>1000
10	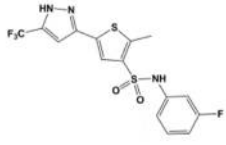	>1000	**16**	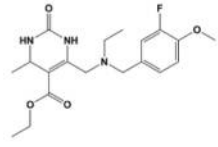	>1000
11	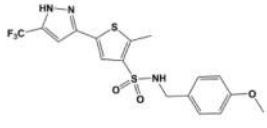	>1000	**17**	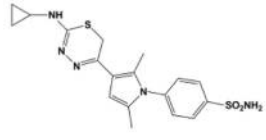	>1000

with **5** (PDB ID: 1KZN). To find molecules that would retain this efficient molecular recognition pattern, we employed several in silico techniques as powerful drug design tools. First, a structure-based pharmacophore model mimicking the

dx.doi.org/10.1021/jm300395d | *J. Med. Chem.* 2012, 55, 6413−6426

Table 2. Inhibitory Activity of the 4,5′-Bithiazole Compounds 6 and 18−25 against Bacterial DNA Gyrase from *E. coli* Selected in Design Phase II

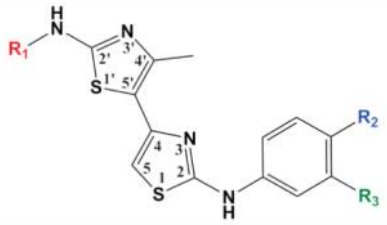

Compd	R_1	R_2	R_3	IC_{50} [μM]
6	$-COCH_3$	-COOH	-H	5.5 ± 1.0
18	$-COCH_2CH_3$	-COOH	-H	1.1 ± 0.2
19	-H	$-SO_2NH_2$	-H	8.2 ± 1.6
20	$-COCH_3$	-OH	-H	30 ± 3
21	-H	-COOH	-OH	67 ± 21
22	-H	-OH	-H	125 ± 18
23	-H	-OH	-COOH	>1000
24	$-COCH_3$	-H	-COOH	>1000
25	$-COCH_3$	$-N(CH_3)_2$	-H	>1000

interactions of **5** with G24 active site environment was generated using LigandScout software[45] consisting of overall 12 pharmacophore features: two hydrogen bond donors, two hydrogen bond acceptors, an aromatic ring, and seven hydrophobic features (see Supporting Information, Figure S1 for the full pharmacophore model). Exclusion volume spheres were also derived, mimicking the G24 protein environment.

To enlarge the chemical space that would be identified by the pharmacophore model and increase the diversity of hits in the virtual screening campaign, this initial pharmacophore was further reduced. The reduced pharmacophore model describing the tentative pattern of the most important interactions for DNA gyrase B inhibition,[21] without exclusion volume spheres that modeled the spatially derived restraints of the active site, is shown in Figure 3A (see Supporting Information, Figure S2 for the reduced pharmacophore model with included exclusion volume spheres). It was composed of the following elements: one hydrogen bond donor modeling the interaction with the Asp73 residue[20] and two hydrogen bond acceptors, one describing the interaction with the Thr165 residue via conserved water molecule (W1001) and the other with the Arg136 residue. Two hydrophobic interactions in the model, the first describing the methyl group of the pyrrole moiety and the pyrrole ring itself and the second which is located in the place of methyl groups of the L-noviose moiety, were both interpolated into two single hydrophobic spheres from previously derived pairs of hydrophobic spheres, and their tolerance was increased in size by 0.3 Å (see Supporting Information, Figure S1 for the initial pharmacophore model). The third hydrophobic sphere was positioned on the coumarin moiety replacing the aromatic sphere. The remaining hydrophobic elements were not considered in the reduced model.

According to standard practice in VS procedures, this pharmacophore model was successfully assessed for its ability to recognize the bioactive conformation of **5** (see Supporting Information, Figure S3). Subsequently, this pharmacophore model was used in the large scale virtual screening campaign, using a database of approximately 5 million commercially available compounds.[46] This procedure resulted in approximately 400 virtual hits from different structural classes that were able to comply with these pharmacophore features. An example of a hit molecule (**6**) from 4,5′-bithiazole class identified by LigandScout is shown (Figure 3B).

Hits obtained in the first crude step of the virtual screening campaign were subsequently docked into the G24 active site using the GOLD[47] molecular docking tool (see Molecular Docking Calculations, section 4.2. for GOLD parameter settings) to explore the possible orientations of these molecules in the ATP-binding site. A successful validation[48] of the docking model was made by redocking the molecule **5** (see Supporting Information, Figure S4) in the ATP-binding site of G24 protein. This binding site was defined as a 10 Å spherical cavity around molecule **5**, and a further constraint was added, defining Asp73 as a hydrogen bond acceptor: the interaction recognized as an essential feature for tight binding in several structural experiments[15,20] and also proficiently used in our previous studies.[43,44] The conserved water molecule, W1001, coordinated with Asp73, Gly77, and Thr165 residues, was included in the docking calculation. Its importance for the successful inhibitor binding was confirmed in previous thermodynamic and structural studies.[49] The docking procedure was performed by applying the GOLDScore scoring function, and all docking solutions were visually inspected for the crucial interactions with the ATP-binding site residues Asp73, Thr165 (through the W1001 water molecule), and Arg136 important for recognition of coumarin inhibitors.[16] Twelve compounds from different structural classes: four bithiazoles (**6**–**9**), two pyrazoles (**10**, **11**), three cyanoacryla-

dx.doi.org/10.1021/jm300395d | J. Med. Chem. 2012, 55, 6413−6426

mides (**12**−**14**), and one triazine (**15**), dihydropyrimidinone (**16**) and thiadiazine(**17**) were selected from a pool of approximately 400 hits by applying previously derived criteria, and their biological activity was determined using a standard DNA gyrase assay (see see Supporting Information, Table S1).[50] The results of the in vitro assay are presented in Table 1. In the first design phase, only two compounds from the class of 4,5′-bithiazole-2,2′-diamines (**6** and **7**) were found to possess antigyrase activity, and one of them (**6**) displayed inhibitory activity in a low micromolar range with the determined IC_{50} value of 5.5 ± 1.0 μM. A variety of enzymes whose activity is coupled with the ATP catalysis (e.g., the large family of protein kinases) would also hypothetically bind the series of 4,5′ bithiazoles. An example of such binding was already observed for the case of phosphoinositide 3-kinase (PI3K).[51]

2.2. Design Phase II: Virtual Screening of a Focused Library of Compounds from the 4,5′-Bithiazole]-2,2′-diamine Chemical Class. The first phase of our VS campaign, described in Section 2.1, yielded a promising low micromolar inhibitor of DNA gyrase from the chemical class of 4,5′-bithiazole molecules. Consequently, a focused library (240 molecules) of 4′-methyl-N^2-phenyl-[4,5′-bithiazole]-2,2′-diamines was extracted from the eMolecules library of commercially available compounds[46] and their initial 3-D structures were generated using OMEGA software.[52] All compounds were docked into the G24 ATP-binding site using GOLD software, and their poses were visually inspected for potential interactions with the amino acids residues of the active site, particularly taking into account the previous selection of residues: Asp73, Thr165 via the conserved W1001 water molecule, and Arg136. Finally, eight commercially available compounds were assayed for their DNA gyrase inhibitory activity (Table 2). Two of the newly purchased compounds (**25** and **26**) had slightly different structural elements, both lacking the hydrogen bond acceptor group on the para position of the phenyl ring, which enabled us to further validate the importance of this interaction and expand the first structure−activity relationship (SAR) analysis. The results of the in vitro DNA gyrase assay are presented in Table 2. All commercially available compounds possessing DNA gyrase activity, **6** and **18**−**22**, were characterized by HR-MS techniques and their purity was determined to be ≥95% by microanalysis. (see Section 4.3. and Supporting Information Section 7).

The inhibition results obtained from both design phases were first analyzed in light of our in silico model. In Figure 4, a GOLD binding conformation of the inhibitor **6** is depicted. Similar interaction pattern was observed throughout the 4,5′-bithiazole series (see Supporting Information, Figure S5 for GOLD-calculated binding modes of compounds **18** and **20**). Results of the docking process predicted the interaction of the amide hydrogen with Asp73 residue and interaction of the 3′ nitrogen of the thiazole ring with the conserved water molecule W1001. This shows that the 2-aminothiazole moiety is able to fulfill the general prerequisite for gyrase inhibition by containing this acceptor−donor interaction pattern and could be considered a promising starting scaffold. As in our previous study,[44] the second thiazole ring appeared to be suitable linker between the first thiazole ring and the substituted phenyl ring and is additionally capable of hydrophobic interactions. Furthermore, the phenyl ring substitution was shown to be of importance, and the hydrogen bond acceptor on the para position of the phenyl ring is apparently crucial for the

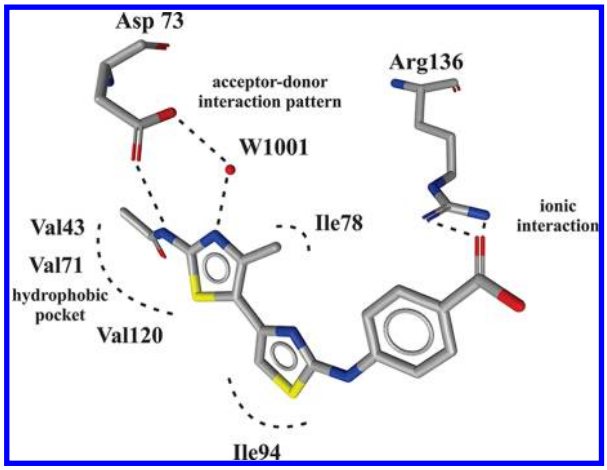

Figure 4. GOLD-calculated binding mode of the VS hit compound **6** docked into the G24 ATP binding site. Amino acid residues Asp73 and Arg136 along with water molecule W1001 important for molecular recognition are depicted. Curved lines represent hydrophobic interactions with residues Val43, Val71, Ile78, Ile94, and Val120, which are omitted in this figure. A similar interaction pattern was observed throughout the active 4,5′-bithiazole series.

inhibitory activity. Both compounds (**24**, **25**) lacking the hydrogen bond acceptor on the para position were found to be inactive (IC_{50} > 1000 μM). Interestingly, the compound **24** having the *p*-hydroxyl substituted phenyl ring was also inactive, which is most probably the consequence of the presence of the carboxyl group at the meta position being unable to form an optimal interaction with the Arg136 residue. The comparison of compounds **6** and **25** also favors this rationale. While compound **6** showed inhibitory activity with an IC_{50} value of 5.5 ± 1.0 μM, compound **24** showed no activity (IC_{50} > 1000 μM), thus postulating that the meta substitution is not only less favorable than the para substitution but it also leads to a complete inactivity. Furthermore, the carboxyl group in position R_2 is preferred over the hydroxyl or acetamido group, which is also in accordance with our model.

The group at the para position of the phenyl ring interacts with the basic guanidyl group of the Arg136 residue (Figure 4). In this case, the carboxyl group is capable of forming additional ionic interaction, which contributes considerably to the strength of binding interactions. Furthermore, in most cases, the 2′-acetyl substitution of the 2′-amino group leads to a higher activity of the inhibitor. The lipophilic part of the 2′ substituent is positioned in the hydrophobic pocket of the ATP-binding site and forms favorable hydrophobic interactions with Val43, Val71, and Val167 residues, the only exception being compounds **7** and **19**, where the latter compound is more active with the IC_{50} of 8.2 ± 1.6 μM. According to our in silico model, the possible reason for this observation is that the presence of the 2′-acetamido group in the case of compound **7** moves the sulfonamido group too far from the Arg136 residue, thus disabling the optimal ionic interaction between the inhibitor and the amino acid residue. The sulfonamido group is apparently too bulky to be incorporated within the protein-active site. In the case of compounds **20** and **22** (IC_{50} of 30 ± 3 μM and 125 ± 18 μM, respectively), the presence of the 2′-acetyl group increases the activity by the factor of 4. The importance of the 2′ substitution is further substantiated by the comparison of compounds **6** and **18** (IC_{50} of 5.5 ± 1.0 and 1.1 ± 0.2 μM, respectively), indicating that the hydrophobic pocket

dx.doi.org/10.1021/jm300395d | J. Med. Chem. 2012, 55, 6413−6426

is large enough to incorporate even a propanoyl group. The addition of another CH_2 group thus increases the inhibitory activity by a factor of 5; however, the hydrophobic pocket is apparently too small to accommodate a benzoyl moiety, which seems to be the main reason for the complete inactivity of compound **8** (IC_{50} > 1000 μM).

All active compounds (**6**, **18**–**22**) were tested for their in vitro antibacterial activity against three bacterial strains: ATCC 29213 from *Staphylococcus aureus*, ATCC 29212 from *Enterococcus faecalis*, and ATCC 49766 from *Haemophilus influenzae* using the protocol as described in Section 4.4. Cefuroxime and gentamicin were included as reference compounds. The results of the antibacterial testing are presented in the Table 3.

Table 3. In Vitro Antibacterial Activity of Selected Compounds from the Class of 4,5′-Bithiazoles (in μg/mL)

compd	*S. aureus* ATCC 29213	*E. faecalis* ATCC 29212	*H. influenzae* ATCC 49766
6	256	128	64
18	>256	256	64
19	>256	256	32
20	>256	256	128
21	256	64	>256
22	64	32	64
Cefuroxime			0,5
Gentamycin	0,5	8	

Compound **22** displayed slight in vitro antibacterial activity against all three bacterial strains, and compounds **6**, **18**, and **19** displayed weak antibacterial activity against the bacterial strain ATCC 49766 from *H. influenzae*. Because *E. coli* bacterial species, which was used in the design stages as well as the in vitro assay of the hit compounds, was not used in the microbiological activity study, comparison of the ATP-binding sites was performed to inspect for potential differences of the ATP binding site. Primary sequences of the DNA gyrase from bacterial species *E. coli*, *S. aureus*, *E. faecalis*, and *H. influenza* were retrieved from the Protein database, freely available at the National Center for Biotechnology Information (NCBI).[53] Multiple sequence alignment was performed using the Clustal Omega program.[54] Results of the alignment procedure are presented in Table S3 of the Supporting Information. The comparison revealed only negligible differences between four bacterial strains. Second, previous investigations[14,15] have shown that the *E. coli* strain appears to be sensitive to similar compounds only in *Tol C* form, i.e., without efflux transporter, and such a strain was not available to us.

2.3. Biophysical and Structural Evaluation of the 4,5′-Bithiazole-2,2′-diamine Chemical Class. *2.3.1. Differential Scanning Fluorimetry (DSF) Experiments.* The active compounds from this novel 4,5′-bithiazole chemical class of molecules were further investigated using different available biophysical techniques. Their ability to stabilize the G24 protein was assessed utilizing the DSF technique by which the thermal stability of the G24 native protein and of the protein complex with the ligand is measured.[55] Complexes with six different ligands (**6**, **18**–**22**) were stepwise heated from 25 to 95 °C in steps of 1 °C in the presence of the fluorescent dye whose fluorescence increases when it interacts with the hydrophobic residues of the protein. These residues become exposed to the dye when the protein is denatured. A higher positive shift of T_m in comparison to native protein means higher stabilization of the complexes, which is a consequence of the inhibitor binding. The results of the obtained melting temperatures are shown in Supporting Information, Table S4.

Two compounds (**6**, **18**) showed significant improvement in the stability of the G24 protein–ligand complex; using our design model, we were able to gain new evidence that the carboxyl group at the para position plays an important role in the complex stabilization by interacting with Arg136, as suggested by our in silico model (Figure 4 and Supporting Information, Figure S5). Furthermore, the lipophilic group that occupies the hydrophobic pocket formed by the residues Val43, Ala47, Val71, Val120, and Val167 also contributes to the stabilization. The best improvement in the protein–inhibitor complex stability was observed in the case of compound **18** with the T_m shift of 5.0 °C, which is in accordance with the most potent DNA gyrase inhibition with IC_{50} of 1.1 ± 0.2 μM. Figure 5 depicts the curves obtained in the DSF experiment for the G24 protein–compound **18** complex (red) compared with the native protein curve (blue).

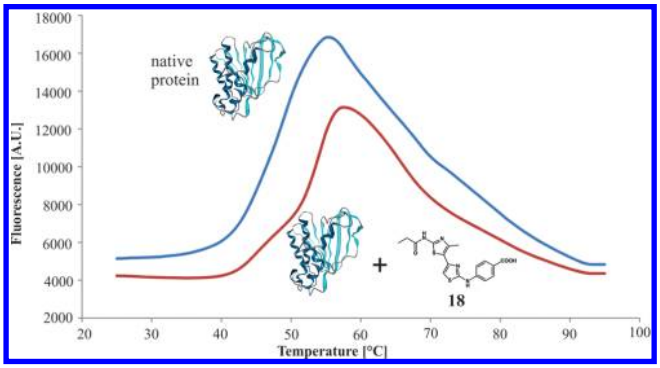

Figure 5. DSF experiment for compound **18** showing an increase in thermal stability between the native G24 protein (blue) and G24 protein–compound **18** complex (red).

2.3.2. Surface Plasmon Resonance (SPR) Experiments. The binding mode of two most active compounds in the DSF experiments (**6**, **18**) was additionally validated with the surface plasmon resonance (SPR) technique used for the characterization of the intermolecular interactions.[56,57] Results of the SPR experiments are presented in Figure 6 and revealed fast and tight binding of inhibitors to the G24 protein at low micromolar concentrations. The G24 protein was immobilized on the CM5 chip, and its activity was tested and confirmed using **1** as a standard (measured K_d of 28 nM in comparison to 19 nM in the literature).[58] Both inhibitors were tested at least eight different concentrations in three parallels depending on the noticeable response of the immobilized protein (see Figure S7 of Supporting Information for obtained sensorgrams of compounds **6** and **18** at different measured concentrations), and the K_d values were determined using Origin software with a steady state affinity binding model (one site binding). K_d values were in good agreement with the previously determined IC_{50} inhibitory activity values. The difference in K_d values clearly shows the importance of the hydrophobic pocket (see Figure 2) occupation as the prolongation by another methyl group resulted in an almost 10 times lower K_d value.

2.3.3. Microscale Thermophoresis (MST) Measurements. K_d values for two molecules **6** and **18** were evaluated by using microscale thermophoresis, an emerging new technique for intermolecular interactions studies.[59] The technique is based on

dx.doi.org/10.1021/jm300395d | J. Med. Chem. 2012, 55, 6413–6426

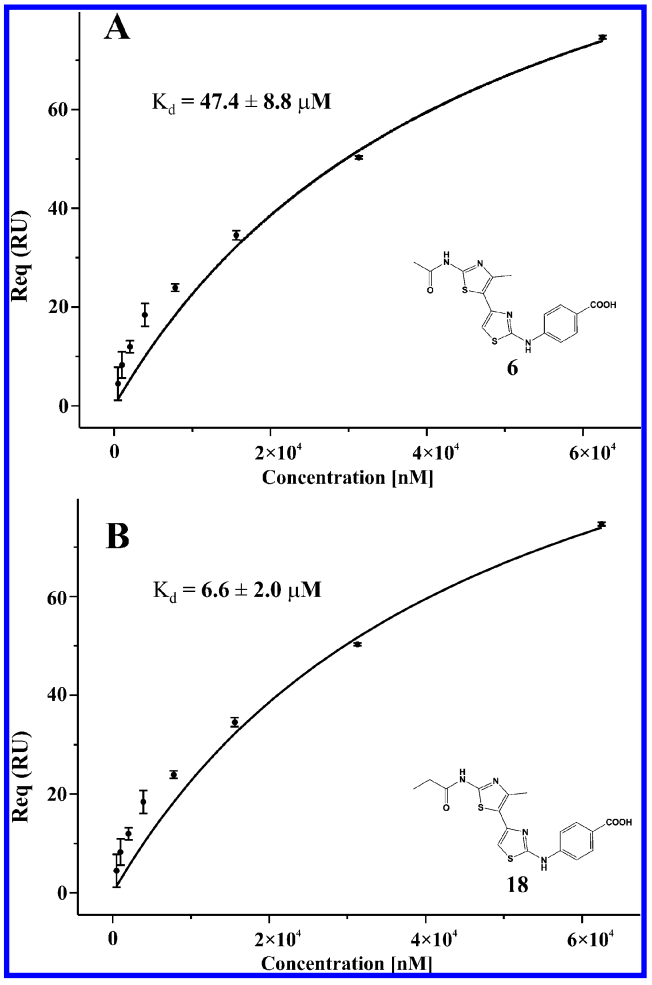

Figure 6. The results of the SPR experiments for compound **6** (A) and compound **18** (B) with the displayed calculated K_d values. RU denotes response units.

the formation of the complex between the fluorescently labeled protein and unlabeled ligand in a solution that is subsequently heated with a laser. Upon heating, the migration of the complex from the heated area occurs and the thermophoretic movement of the fluorescently labeled molecule is measured by monitoring the fluorescence distribution (F) inside a capillary. The measurement signal directly corresponds to the fraction of the bound molecules (see Figure S8 of Supporting Information for the obtained thermogram plots), and K_d values are calculated from the law of mass action. They were obtained by fitting the binding curve with the quadratic solution for the fraction of bound molecules (Figure 7). The K_d values for compounds **6** (Figure 7A) and **18** (Figure 7B) were 51.1 and 7.9 μM, respectively, which is in reasonable agreement with the previously determined values from the SPR experiments.

*2.3.4. Structural Analysis of the G24 Protein Complex with Compound **18**.* As the compounds **6** and **18** showed the strongest inhibitory activity to the G24 protein, they were further used in the crystallization experiments to determine the structure of the G24 ligand complex, provide crucial structural information for further optimization, and possibly enhance our early in silico design steps via direct validation. Extensive initial trials revealed some promising starting conditions, and after the optimization process, crystals of the complexes between G24 subunit and compound **6** and **18** were grown in 0.1 M MES (pH 6.4), 0.2 M $NaNO_3$, and 22% PEG 3350 over a period of two days. Unfortunately, only crystals of the G24 protein cocrystallized with the inhibitor **18** (see Figure S10 of Supporting Information) were of sufficient size and diffraction quality to yield adequate diffraction data, collected in a Bessy synchrotron (Berlin, Germany).

The atomic structure of DNA gyrase B fragment was similar to previously published structure[16] (rmsd for 182 aligned CA atoms between 1KZN and our structure is 0.50 Å and 0.71 Å for molecule A and B in asymmetric unit, respectively). However, due to the improved resolution of 1.5 Å (when compared to the previously solved closed structures of *E. coli* G24 complex with different inhibitors),[16] we were able to place residues 97−108 from the flexible loop region,[60] which were

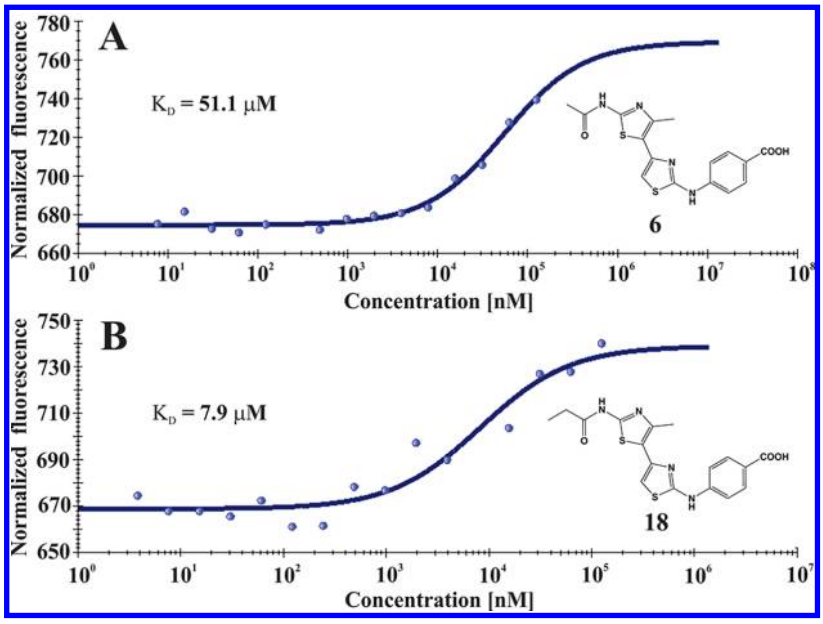

Figure 7. MST experimental values for compounds **6** (A) and **18** (B) fitted on the binding curve.

dx.doi.org/10.1021/jm300395d | *J. Med. Chem.* 2012, 55, 6413−6426

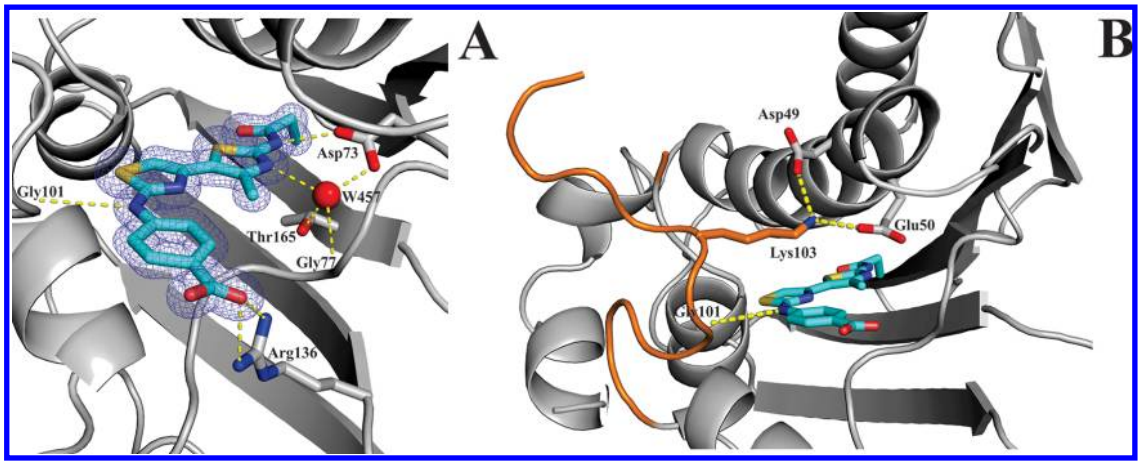

Figure 8. (A) The position of the compound **18** in the active site of G24. Hydrogen bonds are presented with dotted lines; electronic density, contoured at 2σ, is shown as meshed net. (B) Interactions stabilizing the flexible loop. Salt bridge formed between Lys103 and Asp49, Glu50 residues, and hydrogen bond between the amine nitrogen of inhibitor and carbonyl group of Gly101 residue.

disordered in previous structures. The position and conformation of the inhibitor in the ATP binding pocket was clearly defined by the electron density, and it was gratifying to observe that in the determined crystal structure the conformation of the 4,5′-bithiazole inhibitor **18** was fully in line with our in silico model. In Figure 8A, the experimentally determined binding mode for compound **18** is depicted within the ATP-binding site. Structural coordinates of the refined model have been deposited in the RCSB Protein Data Bank under the accession code 4DUH.

The amide hydrogen of the 2′-propionylamido group forms a direct hydrogen bond with the Asp73 residue, and the heterocyclic 3′ nitrogen of the thiazole ring interacts with the conserved W457 water molecule, which corresponds to W1001 in the 1KZN structure, and is further coordinated with the Asp73, Gly77, and Thr165 residues. These two H-bonds, both of the length 2.8 Å, together form the classical hydrogen bond donor−acceptor interaction pattern representative for the majority of DNA gyrase inhibitors.[10,37] The para carboxylic group on the phenyl ring forms two hydrogen bonds of 2.9 Å lengths with the Arg136 residue as well as an additional ionic interaction with this residue. Hydrophobic interactions between the G24 protein and the inhibitor are formed by the propionyl moiety, which sits in the hydrophobic pocket formed by the Val43, Val71, Val120, and Val167 residues, and the 4′-methyl group, which is placed in the position of the chlorine atom of **5** and interacts with Ile78 residue. The second thiazole ring, which occupies the space where methyl groups of the sugar part of coumarin inhibitors are placed, interacts with Ile78, Ile94, and Val120 hydrophobic residues (Figure 8A).

An additional hydrogen bond was located between the 2-amino hydrogen and Gly101 carbonyl oxygen (Figure 8A,B). As glycine Gly101 is already a part of the flexible loop, its interaction with the inhibitor most probably stabilizes the loop, decreases its flexibility, and enhances chances for successful crystallization as well as contributing to the enhanced binding. Interestingly, several hydrophobic interactions with this loop were described in the structure of the pyrrazolothiazole inhibitor−G24 complex.[14] This flexible loop, which was extensively studied using computational approaches,[60] was additionally stabilized with the ionic interaction between Lys103 residue from the loop and acidic residues Asp49 and Glu50 (see Figure 8B and Supporting Information, Figure S11). Lys103 plays a significant role in the binding of the natural substrate ATP as observed in the native protein crystal structure.[9] It is important to note that our previous attempts to obtain crystals of complexes with inhibitors lacking this interaction did not meet with success. Inhibitor **18** showed noteworthy stabilizing effect on the complex with G24 protein as observed by DSF (Supporting Information, Table S3).

It should be noted that performing X-ray studies on the G43 fragment (gyrase B 43 kDa domain) of the DNA gyrase in complex with the inhibitors would even further improve the understanding of contacts with ATP binding site because it takes into account the dimeric active form of the enzyme. However, by using the G24 protein, a direct structural comparison of the starting compound **5** in complex with G24 and inhibitor **18** is possible.

To compare the experimental binding mode with our in silico model, which was used in both design stages, we redocked compound **18** in the 4DUH structure using the same procedure as described previously. The result of the docking calculation is shown in Figure 9. The rms value between the experimental (gray) and calculated (black) binding mode was 0.59 Å, confirming the appropriateness of our design model and value for further drug design implementation. In addition,

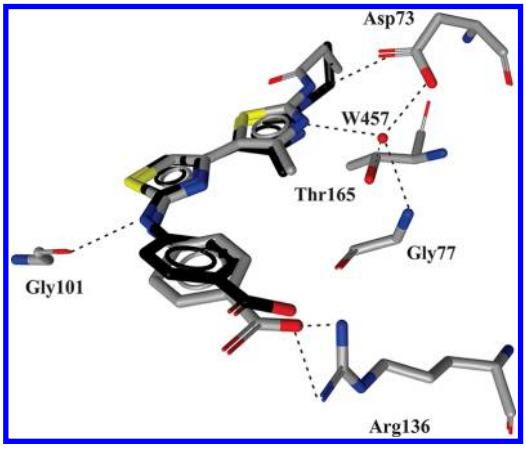

Figure 9. Comparison of experimentally determined (gray) and redocked (black) positions of the compound **18** in the 4DUH active site.

dx.doi.org/10.1021/jm300395d | J. Med. Chem. 2012, 55, 6413−6426

1KZN and 4DUH structures were superimposed and rmsd value between GOLD-calculated binding modes of compound **18** in both protein structures was calculated. Only negligible influence of the G24 protein structure on the generated docked conformations of compound **18** was observed (see Supporting Information, Figure S6).

3. CONCLUSION

In our continuous efforts to discover novel compounds with antigyrase activity,[10,35,36,43,44] the identification and characterization of a novel class of 4′-methyl-N^2-phenyl-[4,5′-bithiazole]-2,2′-diamine bacterial gyrase inhibitors within a low range of micromolar activity (best active compound **18** with IC_{50} of 1.1 ± 0.2 μM) is described. By utilizing a combination of in silico, biophysical, and structural techniques[43,44] starting from the available structural data of the natural inhibitor **5** from the coumarin class, a structure-based pharmacophore model for the description of crucial ligand interactions was constructed, yielding six active compounds of the 4,5-bithiazole structural class. They were found to be low micromolar in vitro DNA gyrase B inhibitors, and their binding mode was additionally characterized using surface plasmon resonance (SPR), microscale thermophoresis (MST), and differential scanning fluorimetry experiments (DSF). It was gratifying to observe that the highest increase of thermal stability of the complex inhibitor **18**−protein G24 matches the best in vitro activity of this compound. The final proof of our design strategy was obtained when the crystal structure of the complex of the G24 protein and compound **18** was solved at 1.5 Å. It showed good agreement between the theoretically predicted and experimentally determined binding mode consequently provoking the advantages of the virtual screening techniques as a powerful tool for the identification of new hit compounds in initial steps of novel antibacterial discovery. In addition, the significance of the inhibitor interaction with the protein loop residue Gly101 was revealed as significant factor in the binding of this compound class. Furthermore, this class of 4,5′-bithiazole compounds encompasses a collection of promising lead compounds for further optimization and development to yield novel drugs aimed to combat ever-present bacterial infections.

4. EXPERIMENTAL SECTION

4.1. Structure-Based Pharmacophore Model Generation and Virtual Screening Procedure. The crystal structure of the complex between G24 DNA gyrase subunit and **5** was retrieved from the Protein Data Bank (PDB code: 1KZN), and interactions were examined using the LigandScout software. Subsequently, a structure-based pharmacophore was derived for **5** (see Supporting Information, Figure S1), and the initial number of pharmacophoric features was reduced to obtain a sufficient molecular recognition pattern required for ligand binding on one hand and to increase the chemical space identified by the pharmacophore model on the other.[16] The final model used for the first phase VS campaign consisted of a hydrogen bond donor, two hydrogen bond acceptors, and three hydrophobic features (Figure 3A). Exclusion volume spheres were also included to take into account the spatial constraints of the G24 protein binding site (see Supporting Information, Figure S2 for model with exclusion volume spheres). The pharmacophore model was according to standard practice in VS[48] successfully validated for its ability to recognize the bioactive conformer of **5** (see Supporting Information, Figure S3 for comparison). These results provided confidence for subsequent virtual screening campaign. The pharmacophore model was screened against 5 million commercially available compounds, all previously converted into multifunctional format (25 conformers for each compound in the database) also using LigandScout as a screening tool. The conformers of molecules in the screening library were generated using idbgen module available in LigandScout coupled with OMEGA software. The default high-throughput settings were used for the library generation (max number of output conformers per molecule = 25, rms threshold to duplicate conformers = 0.8 Å, max number of all generated conformers per molecule = 30000, max number of intermediate conformers per molecule = 4000).

4.2. Molecular Docking Calculations. Molecular docking calculations were performed using GOLD docking tool.[47] To begin with, the docking software tool GOLD was validated.[48] For this purpose, initial conformation of the molecule **5** within the G24 active site (PDB: 1KZN) was extracted from its active site and subsequently docked using the GOLD molecular docking package (Supporting Information, Figure S4).[47] The ATP binding site was defined as a 10 Å cavity around **5**, and a docking constrain defining Asp73 as a hydrogen bond acceptor was added.[17,20] Because of its importance revealed by several structural studies, the water molecule W1001 located in the ATP-active site was included in the GOLD docking studies.[49] In the validation procedure molecule **5** was docked 10 times into the defined binding site by applying the following parameters of the GOLD genetic algorithm (GA) (population size = 100, selection pressure = 1.1, no. of operations = 100000, no. of islands = 5, niche size = 2, migrate = 10, mutate = 95, crossover = 95) and several different scoring functions (GOLDscore, CHEMscore, and ASP). The best agreement between the crystallized and docked pose was obtained using GoldScore scoring function (rms of 0.55 Å, see Supporting Information, Figure S4), which comprised of four components (protein−ligand hydrogen bond energy, protein−ligand van der Waals energy, ligand internal van der Waals energy, and ligand torsional strain energy), and it was used further for the molecular docking calculations of the selected compounds in both design stages. These GOLD parameters were also used in docking of the bithiazole focused library and redocking study of the inhibitor **18** into our newly solved 4DUH crystal structure.

4.3. In Vitro Screening of the Selected Hit Compounds for Inhibitory Activity and Determination of IC_{50} Values. The assay for the determination of IC_{50} values (Inspiralis) was performed on the black streptavidin-coated 96-well microtiter plates.[50] The plate was first rehydrated with the supplied wash buffer (20 mM Tris-HCl (pH 7.6), 137 mM NaCl, 0.01% (w/v) BSA, 0.05% (v/v) Tween 20) and biotinylated oligonucelotide was immobilized onto the wells. The excess of oligonucleotide was then washed off, and the enzyme assay was carried out in the wells. The final reaction volume of 30 μL contained 1.5 U of gyrase from *E. coli*, 1 μg of relaxed pNO1 plasmid, and 0.3 μL of inhibitors stock solution in DMSO. Reactions were incubated for 30 min at 37 °C and after the addition of the TF buffer (50 mM NaOAc pH 5.0, 50 mM NaCl and 50 mM $MgCl_2$) which terminated the enzymatic reaction for another 30 min at room temperature to allow the triplex formation (biotin−oligonucleotide−plasmid). Afterward, the unbound plasmid was washed off and the solution of SybrGOLD stain in T10 buffer (10 mM Tris-HCl pH 8.0 and 1 mM EDTA) was added. After mixing the fluorescence (excitation, 485 nm; emission, 535 nm) was read using a Tecan fluorimeter. Preliminary screening was performed at inhibitor concentrations of 500, 125, 31.3, and 7.8 μM, respectively. All actives were further tested at 250, 62.5, 15.6, and 3.9 μM, and those showing significant activity at 3.9 μM were also tested at 2, 1, 0.5, 0.25, and 0.125 μM depending on their activity at 3.9 μM. IC_{50} values were calculated using GraphPad Prism software and represent the concentration of inhibitor where the residual activity of the enzyme is 50%. Obtained results are presented in Tables 1 and 2. All commercially available compounds possessing DNA gyrase activity (**6**, **18**−**22**) were characterized by HR-MS technique, and their purity was determined by microanalysis performed on a Perkin-Elmer C, H, N, S analyzer using a modified Pregl−Dumas method. Analyses indicated that all elements were within 0.4% of the theoretical values. The purity of the tested compound was established to be ≥95% (see Supporting Information, Section 8).

4.4. Antibacterial Activity Measurements. The antibacterial activity study for compounds **6** and **18**–**22** was performed at the Department of Microbiological Surveillance and Research, Statens Serum Institute in Copenhagen, Denmark. Fresh overnight colonies from 5% horse blood agar plates or chocolate agar plates were suspended to a turbidity of 0.5 McFarland and further diluted 1:100 in MH or HTM broth. Then 1024 mg/mL stock solutions of tested compound were prepared in DMSO, and stock solutions of standards (gentamicin, cefuroxime) were prepared in sterile water. To all microtiter plates were added 50 μL of MH/DMSO (*S. aureus* and *E. faecalis*) or HTM/DMSO (*H. influenze*). For control compounds, only broth without DMSO was added. Then 50 μL of relevant solutions were added to the first row and then diluted 1:1. A total of 50 μL of diluted bacterial suspension was added to wells containing 50 μL of 2-fold compound dilutions. Test range was 256–0.25 μg/mL. The plates were incubated at 35 °C in ambient air for 16–20 h for *S. aureus* and *E. faecalis* and 20–24 h for *H. influenzae*. Colony counts of the used inoculum were correct, i.e., 1 $\times 10^6$ CFU/mL, and all control compounds were within the limits according to CLSI. All experiments were performed in triplicate, and the results, MIC in μg/mL, are shown in Table 3.

4.5. DNA Gyrase B 24 kDa Domain Protein Expression and Purification. The 24 kDa domain protein was prepared according to previously published procedure.[36] The overnight culture of the *E. coli* bacteria was grown for 12 h in Lysogeny broth (LB) media containing 150 μg/mL ampicillin at 37 °C with shaking (160 rpm). The culture was inoculated in 4 × 0.5 L LB media (150 μg/mL of ampicillin) and grown in the same conditions until the starting optical density of 0.1 reached the value of 0.5–0.7. The protein expression was induced with the addition of 0.4 mM IPTG, and bacteria were grown for additional 3 h. After the expression, the cells were harvested by centrifugation (5500 rpm, 4 °C, 10 min) and suspended in lysis buffer containing 0.1% deoxycholic acid. The mixture was further sonified (amplitude 40%, 1 s on, 2 s off for 3 min) and centrifuged (12000 rpm, 4 °C, 15 min). To the supernatant, a 20% streptomycin sulfate solution was added stepwise until the final concentration of 4% was reached to eliminate the DNA, and the dispersion was removed by additional centrifugation (12000 rpm, 4 °C, 15 min). The supernatant containing G24 protein was loaded onto a sepharose–novobiocin column, and the protein was purified using affinity chromatography. Each loaded fraction was washed with 50 mL of 20 mM Tris-HCl (pH 8.0), 0.5 M NaCl, 25 mL of 100 mM NaAc (pH 4.0), 0.5 M NaCl, and again 50 mL of Tris-HCl buffer. Protein was eluted with 8 M urea in 20 mM Tris-HCl (pH 7.5). Dialysis was performed 5 times overnight against Tris buffer (20 mM Tris-HCl pH 7.5, 1 mM EDTA, 2 mM DTT), and dialyzed protein was concentrated (3000 rpm, 4 °C) to the final concentration of 10 mg/mL. The purity of the protein was analyzed by SDS PAGE method. A volume of a protein fraction containing approximately 10 μg of G24 protein was applied on the polyacrylamide gel (1 mm, 12%), and 3 μL of a commercially available protein molecular weight marker were added. The electrophoresis was run for a period of 90 min at a constant voltage. The gel was afterward transferred to a solution of Coomassie Brilliant Blue dye in 20% acetic acid. After 15 min of incubation, it was washed several times with the 10% acetic acid in 30% ethanol until the complete transparency of the gel was achieved. The purity of the protein was determined to be >95% for each fraction as only single brands corresponding to the molecular mass between 17 and 28 kDa were observed (see Supporting Information, Figure S9)

4.6. Differential Scanning Fluorimetry (DSF) Experiments. After the initial optimization, the optimal conditions 15 μL of G24 protein (2 mg/mL), 5 μL of dye (SyproOrange, 1:100), and 10 μL of buffer (50 mM Tris-HCl pH 7.4, 2 mM EDTA) were established. In inhibitor test, 3 μL of inhibitor in 1% DMSO (2.5 mM) were added. The solutions were mixed and centrifuged and stepwise heated from 25 to 95 °C (1 °C/min). The fluorescence, which rises when the protein is denatured and hydrophobic amino acid residues are exposed to the dye, was measured three times every minute. Data were processed using DSF spreadsheet, and T_m values were calculated by fitting to the Boltzmann equation using Grafit.[55] All the experiments were performed in three parallels, and changes of T_m between the native protein and the complex were calculated. The results are presented in the Supporting Information, Table S3.

4.7. Surface Plasmon Resonance (SPR) Measurements. Surface plasmon resonance (SPR) measurements for the compounds **6** and **18** were performed on a BiacoreX machine using CM5 sensor chip (Biacore, GE Healthcare). The system was primed twice with running buffer (10 mM Hepes pH 7.4, 150 mM NaCl, 3 mM EDTA, 0.005% surfactant P20). The G24 protein was immobilized on the second flow cell of a sensor chip CM5 using standard amino coupling method. Briefly, the carboxymethylated dextran layer was activated with a 7 min pulse of 1-ethyl-3-(3-dimethylaminopropyl)-carbodiimide (EDC) and *N*-hydroxy succinimide (NHS) mixed in a 1:1 ratio.[56] Protein was diluted to the final concentration of 50 μg/mL in 10 mM sodium acetate (pH 4.5) and injected in two short pulses to reach the final immobilization level around 17400 response units. Finally, the rest of the surface was deactivated with 7 min injection of ethanolamine. The first flow cell was activated with EDC/NHS and deactivated with ethanolamine and served as a reference cell for subtraction of nonspecific binding. Analytes were prepared as DMSO 100× stock solutions and were diluted with a running buffer prior to the injection. They were injected at a flow rate of 30 μL/min for 90 s, and dissociation was monitored for additional 120 s. As the dissociation of analytes from the ligand was rapid, no regeneration protocol was needed. For the titration of analytes, the 1% of the DMSO was added to the running buffer in order to diminish the difference in a refractive index between the samples and running buffer.[56]

Both active compounds **6** and **18** were tested at at least eight different concentrations (depending on their solubility) in three parallel titrations. Some of the concentrations were injected several times to check for the reproducibility of the binding. The sensorgrams (see Supporting Information, Figure S7) were analyzed using BiaEval software (Biacore, GE Healthcare). The equilibrium binding responses were determined from the binding levels 5 s before the stop of the injection. K_d values were determined by the fitting of the data to 1:1 steady state binding model as described in results.

4.8. Miocroscale Thermophoresis (MST) Experiments. The G24 protein was first labeled with the commercially available NT-647 dye using NanoTemper's Protein Labeling Kit RED (no. L001, NanoTemper Technologies). The thermophoretic movement of the fluorescently labeled protein in complex with selected inhibitors (compounds **6** and **18**) was measured by monitoring the fluorescence distribution inside the capillary. The concentration of the labeled protein was kept constant at ∼20 nM concentration, while the concentration of the compound was varied from 125 μM, which was further diluted to 1:1 15 times. The samples were loaded into standard treated MST-grade glass capillaries. The intensities of the LED and laser were 90% and 80%, respectively. After a short incubation period, the MST analysis was performed using the Monolith NT.115. Experimental thermograms are available in Supporting Information, Figure S8.

4.9. 24 kDa *N*-Terminal Part of the GyrB Subunit Crystallization and Data Collection. The protein was concentrated to 10 mg/mL in 20 mM Tris-HCl buffer (pH 7.5), 3 mM EDTA, and 2.5 mM of compound **18**. Crystals were grown in 100 mM MES (pH 6.4), 22% PEG 3350, and 0.2 M $NaNO_3$ by the sitting drop method in a period of two days. The diffraction data was collected at PX14.1 workstation at synchrotron Bessy (Berlin, Germany). The data were processed using HKL2000 package.[61] The structure was determined by molecular replacement with Phaser[62] using DNA gyrase (PDB ID: 1KZN) as a search model. The structure was refined with Refmac[63] and MAIN.[64] Geometric parameters for compound **18** were obtained from Pury server.[65] The data collection and refinement statistics is summarized in Table 4.

Table 4. X-ray Data Collection and Refinement Statistic

	4DUH
space group	$P2_1$
Cell Dimensions	
a (Å)	53.24
b (Å)	51.12
c (Å)	79.13
α (deg)	90.00
β (deg)	95.68
γ (deg)	90.00
resolution (Å)	20−1.5
R_{merge} (%)	5.1 (47.6)
$I/\sigma I$	49.5 (4.0)
completeness (%)	99.2 (83.3)
redundancy	7.3 (7.1)
Refinement	
resolution	20−1.50
no. of reflections (work/free)	60619/3420
R_{work}/R_{free}	19.1/22.5
rms deviation	
bond lengths (Å)	0.018
bond angles (deg)	1.53

■ ASSOCIATED CONTENT

Supporting Information

Complete list of assayed compounds, structure-based pharmacophore model generation, optimization, and validation, GOLD molecular docking tool validation and docking experiments, multiple sequence alignment of DNA gyrase B primary sequences, differential scanning fluorimetry (DSF) results, surface plasmon resonance (SPR) sensorgrams, microscale thermophoresis (MST) thermograms, NMR characterization of active compounds, results of HR-MS analysis and elemental analysis data, protein purity identification process, G24 protein−compound **18** complex crystals, and additional findings about the flexible loop conformation. This material is available free of charge via the Internet at http://pubs.acs.org.

Accession Codes

The PDB accession code for the G24−**18** complex is 4DUH.

■ AUTHOR INFORMATION

Corresponding Author

*For T.S.: phone, +386-1-4760-277; fax, +386-1-4760-200; E-mail, tom.solmajer@ki.si. For A.P.: phone, +386-1-4760-376; fax, +386-1-4760-200; E-mail, andrej.perdih@ki.si.

Notes

The authors declare no competing financial interest.

■ ACKNOWLEDGMENTS

This work was supported by the Ministry of Higher Education, Science and Technology of the Republic of Slovenia, grant J1-308 to T.S., Young Researcher Grant 1000-08-310063 to M.B., postdoctoral grant Z1-4111 to A.P., structural biology grant P-0048 and infrastructural grant for the Center for Protein Production and Structure at JSI. We are sincerely grateful to Prof. Roman Jerala and Robert Bremšak (National Institute of Chemistry, Laboratory of Biotechnology) for help with expression and purification of the G24 protein. We thank the Laboratory of Biomolecular Structure at the National Institute of Chemistry for sharing their laboratory capacities. We sincerely thank Assist. Prof. Lucija Peterlin Mašič (Faculty of Pharmacy, Ljubljana), Dr. Marjetka Podobnik (National Institute of Chemistry, Laboratory for Biosynthesis and Biotransformations), and Prof. Salam Al-Karadaghi (Kemicentrum, Department of Biochemistry and Structural Biology, Lund University) for stimulating discussions in the initial phase of this work. Dr. Stephen Blanke (NanoTemeper Technologies, Munich, Germany) is kindly acknowledged for his kind assistance with the MST measurements. We thank Vesna Hodnik (Department of Biology, Biotechnical Faculty, University of Ljubljana) for her technical assistance and Amrita Roy Choudhury (National Institute of Chemistry, Laboratory of Chemometrics) for her help with multiple protein sequence alignment. Terry Jackson is acknowledged for his editing contribution to the manuscript.

■ ABBREVIATIONS USED

DNA, DNA; Gyr, gyrase; GyrA, A subunit of the DNA gyrase; GyrB, B subunit of the DNA gyrase; ATP, adenosine triphosphate; NVB, novobiocin; CBN, clorobiocin; HTS, high throughput screening; VS, virtual screening; MIC, minimal inhibitory concentration; SPR, surface plasmon resonance; MST, microscale thermophoresis; DSF, differential scanning fluorimetry; SAR, structure−activity relationship

■ REFERENCES

(1) Brown, E. D.; Wright, G. D. New targets and screening approaches in antimicrobial drug discovery. *Chem. Rev.* **2005**, *105*, 759−774.

(2) Silver, L. L. Does the cell wall of bacteria remain a viable source of targets for novel antibiotics? *Biochem. Pharmacol.* **2006**, *71*, 996−1005.

(3) Perdih, A.; Kovac, A.; Wolber, G.; Blanot, D.; Gobec, S.; Solmajer, T. Discovery of novel benzene 1,3-dicarboxylic acid inhibitors of bacterial MurD and MurE ligases by structure-based virtual screening approach. *Bioorg. Med. Chem. Lett.* **2009**, *19*, 2668−2673.

(4) Maxwell, A. DNA gyrase as a drug target. *Trends Microbiol.* **1997**, *5*, 102−109.

(5) Collin, F.; Karkare, S.; Maxwell, A. Exploiting bacterial DNA gyrase as a drug target: current state and perspectives. *Appl. Microbiol. Biotechnol* **2011**, *92*, 479−497.

(6) Champoux, J. J. DNA topoisomerases: Structure, function, and mechanism. *Annu. Rev. Biochem.* **2001**, *70*, 369−413.

(7) Jacoby, G. A. Mechanisms of resistance to quinolones. *Clin. Infect. Dis.* **2005**, *41* (Suppl 2), S120−S126.

(8) Minovski, N.; Perdih, A.; Solmajer, T. Combinatorially-generated library of 6-fluoroquinolone analogs as potential novel antitubercular agents: a chemometric and molecular modeling assessment. *J. Mol. Model.* **2012**, *18*, 1735−1753.

(9) Maxwell, A.; Lawson, D. M. The ATP-binding site of type II topoisomerases as a target for antibacterial drugs. *Curr. Top. Med. Chem.* **2003**, *3*, 283−303.

(10) Oblak, M.; Kotnik, M.; Solmajer, T. Discovery and development of ATPase inhibitors of DNA gyrase as antibacterial agents. *Curr. Med. Chem.* **2007**, *14*, 2033−2047.

(11) Garry, M. W. A clinical evaluation of the parenteral use of novobiocin. *Am. J. Med. Sci.* **1958**, *236*, 330−335.

(12) Lamour, V.; Hoermann, L.; Jeltsch, J. M.; Oudet, P.; Moras, D. Crystallization of the 43 kDa ATPase domain of *Thermus thermophilus* gyrase B in complex with novobiocin. *Acta. Crystallogr., Sect. D: Biol. Crystallogr.* **2002**, *58*, 1376−1378.

(13) Lafitte, D.; Lamour, V.; Tsvetkov, P. O.; Makarov, A. A.; Klich, M.; Deprez, P.; Moras, D.; Briand, C.; Gilli, R. DNA gyrase interaction with coumarin-based inhibitors: the role of the hydroxybenzoate

isopentenyl moiety and the 5′-methyl group of the noviose. *Biochemistry* **2002**, *41*, 7217−7223.
(14) Ronkin, S. M.; Badia, M.; Bellon, S.; Grillot, A. L.; Gross, C. H.; Grossman, T. H.; Mani, N.; Parsons, J. D.; Stamos, D.; Trudeau, M.; Wei, Y. Y.; Charifson, P. S. Discovery of pyrazolthiazoles as novel and potent inhibitors of bacterial gyrase. *Bioorg. Med. Chem. Lett.* **2010**, *20*, 2828−2831.
(15) Sherer, B. A.; Hull, K.; Green, O.; Basarab, G.; Hauck, S.; Hill, P.; Loch, J. T.; Mullen, G.; Bist, S.; Bryant, J.; Boriack-Sjodin, A.; Read, J.; DeGrace, N.; Uria-Nickelsen, M.; Illingworth, R. N.; Eakin, A. E. Pyrrolamide DNA gyrase inhibitors: optimization of antibacterial activity and efficacy. *Bioorg. Med. Chem. Lett.* **2011**, *21*, 7416−7420.
(16) Tsai, F. T. F.; Singh, O. M. P.; Skarzynski, T.; Wonacott, A. J.; Weston, S.; Tucker, A.; Pauptit, R. A.; Breeze, A. L.; Poyser, J. P.; OBrien, R.; Ladbury, J. E.; Wigley, D. B. The high-resolution crystal structure of a 24 kDa gyrase B fragment from *E. coli* complexed with one of the most potent coumarin inhibitors, clorobiocin. *Proteins* **1997**, *28*, 41−52.
(17) Gormley, N. A.; Orphanides, G.; Meyer, A.; Cullis, P. M.; Maxwell, A. The interaction of coumarin antibiotics with fragments of the DNA gyrase B protein. *Biochemistry* **1996**, *35*, 5083−5092.
(18) Gilbert, E. J.; Maxwell, A. The 24 kDa N-Terminal Subdomain of the DNA Gyrase-B Protein Binds Coumarin Drugs. *Mol. Microbiol.* **1994**, *12*, 365−373.
(19) Ali, J. A.; Jackson, A. P.; Howells, A. J.; Maxwell, A. The 43-Kilodalton N-Terminal Fragment of the DNA Gyrase-B Protein Hydrolyzes Atp and Binds Coumarin Drugs. *Biochemistry* **1993**, *32*, 2717−2724.
(20) Lewis, R. J.; Singh, O. M. P.; Smith, C. V.; Skarzynski, T.; Maxwell, A.; Wonacott, A. J.; Wigley, D. B. The nature of inhibition of DNA gyrase by the coumarins and the cyclothialidines revealed by X-ray crystallography. *EMBO J.* **1996**, *15*, 1412−1420.
(21) Holdgate, G. A.; Tunnicliffe, A.; Ward, W. H. J.; Weston, S. A.; Rosenbrock, G.; Barth, P. T.; Taylor, I. W. F.; Pauptit, R. A.; Timms, D. The entropic penalty of ordered water accounts for weaker binding of the antibiotic novobiocin to a resistant mutant of DNA gyrase: a thermodynamic and crystallographic study. *Biochemistry* **1997**, *36*, 9663−9673.
(22) Schio, L.; Chatreaux, F.; Loyau, V.; Murer, M.; Ferreira, A.; Mauvais, P.; Bonnefoy, A.; Klich, M. Fine tuning of physicochemical parameters to optimize a new series of novobiocin analogues. *Bioorg. Med. Chem. Lett.* **2001**, *11*, 1461−1464.
(23) Bell, W.; Block, M. H.; Cook, C.; Grant, J. A.; Timms, D. Design, synthesis and evaluation of a novel series of spiroketals based on the structure of the antibacterial gyrase inhibitor novobiocin. *J. Chem. Soc., Perkin Trans 1* **1997**, 2789−2801.
(24) Ferroud, D.; Collard, J.; Klich, M.; Dupuis-Hamelin, C.; Mauvais, P.; Lassaigne, P.; Bonnefoy, A.; Musicki, B. Synthesis and biological evaluation of coumarincarboxylic acids as inhibitors of gyrase B. L-Rhamnose as an effective substitute for L-noviose. *Bioorg. Med. Chem. Lett.* **1999**, *9*, 2881−2886.
(25) Nakada, N.; Shimada, H.; Hirata, T.; Aoki, Y.; Kamiyama, T.; Watanabe, J.; Arisawa, M. Biological Characterization of Cyclothialidine, a New DNA Gyrase Inhibitor. *Antimicrob. Agents Chemother.* **1993**, *37*, 2656−2661.
(26) Oram, M.; Dosanjh, B.; Gormley, N. A.; Smith, G. V.; Fisher, L. M.; Maxwell, A.; Duncan, K. Mode of action of GR122222X, a novel inhibitor of bacterial DNA gyrase. *Antimicrob. Agents Chemother.* **1996**, *40*, 473−476.
(27) Nakada, N.; Gmunder, H.; Hirata, T.; Arisawa, M. Characterization of the Binding-Site for Cyclothialidine on the B-Subunit of DNA Gyrase. *J. Biol. Chem.* **1995**, *270*, 14286−14291.
(28) Rudolph, J.; Theis, H.; Hanke, R.; Endermann, R.; Johannsen, L.; Geschke, F. U. *seco*-Cyclothialidines: new concise synthesis, inhibitory activity toward bacterial and human DNA topoisomerases, and antibacterial properties. *J. Med. Chem.* **2001**, *44*, 619−626.
(29) Angehrn, P.; Buchmann, S.; Funk, C.; Goetschi, E.; Gmuender, H.; Hebeisen, P.; Kostrewa, D.; Link, H.; Luebbers, T.; Masciadri, R.; Nielsen, J.; Reindl, P.; Ricklin, F.; Schmitt-Hoffmann, A.; Theil, F. P. New antibacterial agents derived from the DNA gyrase inhibitor cyclothialidine. *J. Med. Chem.* **2004**, *47*, 1487−1513.
(30) Angehrn, P.; Goetschi, E.; Gmuender, H.; Hebeisen, P.; Hennig, M.; Kuhn, B.; Luebbers, T.; Reindl, P.; Ricklin, F.; Schmitt-Hoffmann, A. A New DNA Gyrase Inhibitor Subclass of the Cyclothialidine Family Based on a Bicyclic Dilactam-Lactone Scaffold. Synthesis and Antibacterial Properties. *J. Med. Chem.* **2011**, *54*, 2207−2224.
(31) Plaper, A.; Golob, M.; Hafner, I.; Oblak, M.; Solmajer, T.; Jerala, R. Characterization of quercetin binding site on DNA gyrase. *Biochem. Biophys. Res. Commun.* **2003**, *306*, 530−536.
(32) Hossion, A. M. L.; Zamami, Y.; Kandahary, R. K.; Tsuchiya, T.; Ogawa, W.; Iwado, A.; Sasaki, K. Quercetin Diacylglycoside Analogues Showing Dual Inhibition of DNA Gyrase and Topoisomerase IV as Novel Antibacterial Agents. *J. Med. Chem.* **2011**, *54*, 3686−3703.
(33) Tanitame, A.; Oyamada, Y.; Ofuji, K.; Fujimoto, M.; Iwai, N.; Hiyama, Y.; Suzuki, K.; Ito, H.; Terauchi, H.; Kawasaki, M.; Nagai, K.; Wachi, M.; Yamagishi, J. Synthesis and antibacterial activity of a novel series of potent DNA gyrase inhibitors. Pyrazole derivatives. *J. Med. Chem.* **2004**, *47*, 3693−3696.
(34) Lubbers, T.; Angehrn, P.; Gmunder, H.; Herzig, S.; Kulhanek, J. Design, synthesis, and structure−activity relationship studies of ATP analogues as DNA gyrase inhibitors. *Bioorg. Med. Chem. Lett.* **2000**, *10*, 821−826.
(35) Oblak, M.; Grdadolnik, S. G.; Kotnik, M.; Jerala, R.; Filipic, M.; Solmajer, T. In silico fragment-based discovery of indolin-2-one analogues as potent DNA gyrase inhibitors. *Bioorg. Med. Chem. Lett.* **2005**, *15*, 5207−5210.
(36) Oblak, M.; Grdadolnik, S. G.; Kotnik, M.; Poterszman, A.; Atkinson, R. A.; Nierengarten, H.; Desplancq, D.; Moras, D.; Solmajer, T. Biophysical characterization of an indolinone inhibitor in the ATP-binding site of DNA gyrase. *Biochem. Biophys. Res. Commun.* **2006**, *349*, 1206−1213.
(37) Boehm, H. J.; Boehringer, M.; Bur, D.; Gmuender, H.; Huber, W.; Klaus, W.; Kostrewa, D.; Kuehne, H.; Luebbers, T.; Meunier-Keller, N. Novel inhibitors of DNA gyrase: 3D structure based biased needle screening, hit validation by biophysical methods, and 3D guided optimization. A promising alternative to random screening. *J. Med. Chem.* **2000**, *43*, 2664−2674.
(38) Charifson, P. S.; Grillot, A. L.; Grossman, T. H.; Parsons, J. D.; Badia, M.; Bellon, S.; Deininger, D. D.; Drumm, J. E.; Gross, C. H.; LeTiran, A.; Liao, Y. S.; Mani, N.; Nicolau, D. P.; Perola, E.; Ronkin, S.; Shannon, D.; Swenson, L. L.; Tang, Q.; Tessier, P. R.; Tian, S. K.; Trudeau, M.; Wang, T. S.; Wei, Y. Y.; Zhang, H.; Stamos, D. Novel dual-targeting benzimidazole urea inhibitors of DNA gyrase and topoisomerase IV possessing potent antibacterial activity: Intelligent design and evolution through the judicious use of structure-guided design and stucture−activity relationships. *J. Med. Chem.* **2008**, *51*, 5243−5263.
(39) East, S. P.; White, C. B.; Barker, O.; Barker, S.; Bennett, J.; Brown, D.; Boyd, E. A.; Brennan, C.; Chowdhury, C.; Collins, I.; Convers-Reignier, E.; Dymock, B. W.; Fletcher, R.; Haydon, D. J.; Gardiner, M.; Hatcher, S.; Ingram, P.; Lancett, P.; Mortenson, P.; Papadopoulos, K.; Smee, C.; Thomaides-Brears, H. B.; Tye, H.; Workman, J.; Czaplewski, L. G. DNA gyrase (GyrB)/topoisomerase IV (ParE) inhibitors: synthesis and antibacterial activity. *Bioorg. Med. Chem. Lett.* **2009**, *19*, 894−899.
(40) Starr, J. T.; Sciotti, R. J.; Hanna, D. L.; Huband, M. D.; Mullins, L. M.; Cai, H.; Gage, J. W.; Lockard, M.; Rauckhorst, M. R.; Owen, R. M.; Lall, M. S.; Tomilo, M.; Chen, H. F.; McCurdy, S. P.; Barbachyn, M. R. 5-(2-Pyrimidinyl)-imidazo[1,2-*a*]pyridines are antibacterial agents targeting the ATPase domains of DNA gyrase and topoisomerase IV. *Bioorg. Med. Chem. Lett.* **2009**, *19*, 5302−5306.
(41) Aboul-Fadl, T.; Abdel-Aziz, H. A.; Abdel-Hamid, M. K.; Elsaman, T.; Thanassi, J.; Pucci, M. J. Schiff Bases of Indoline-2,3-dione: Potential Novel Inhibitors of Mycobacterium Tuberculosis (Mtb) DNA Gyrase. *Molecules* **2011**, *16*, 7864−7879.
(42) Lubbers, T.; Angehrn, P.; Gmunder, H.; Herzig, S. Design, synthesis, and structure−activity relationship studies of new phenolic DNA gyrase inhibitors. *Bioorg. Med. Chem. Lett.* **2007**, *17*, 4708−4714.

(43) Brvar, M.; Perdih, A.; Hodnik, V.; Renko, M.; Anderluh, G.; Jerala, R.; Solmajer, T. In silico discovery and biophysical evaluation of novel 5-(2-hydroxybenzylidene) rhodanine inhibitors of DNA gyrase B. *Bioorg. Med. Chem.* **2012**, *20*, 2572−2580.
(44) Brvar, M.; Perdih, A.; Oblak, M.; Masic, L. P.; Solmajer, T. In silico discovery of 2-amino-4-(2,4-dihydroxyphenyl)thiazoles as novel inhibitors of DNA gyrase B. *Bioorg. Med. Chem. Lett.* **2010**, *20*, 958−962.
(45) Wolber, G.; Langer, T. LigandScout: 3-D pharmacophores derived from protein-bound ligands and their use as virtual screening filters. *J. Chem. Inf. Model.* **2005**, *45*, 160−169.
(46) *eMolecules*; eMolecules, Inc.: Solana Beach, CA; www.emolecules.com (Accessed November 15, 2011).
(47) Jones, G.; Willett, P.; Glen, R. C.; Leach, A. R.; Taylor, R. Development and validation of a genetic algorithm for flexible docking. *J. Mol. Biol.* **1997**, *267*, 727−748.
(48) Kirchmair, J.; Markt, P.; Distinto, S.; Wolber, G.; Langer, T. Evaluation of the performance of 3D virtual screening protocols: RMSD comparisons, enrichment assessments, and decoy selection—what can we learn from earlier mistakes? *J. Comput.-Aided. Mol. Des.* **2008**, *22*, 213−228.
(49) Yu, H.; Rick, S. W. Free energies and entropies of water molecules at the inhibitor−protein interface of DNA gyrase. *J. Am. Chem. Soc.* **2009**, *131*, 6608−6613.
(50) Maxwell, A.; Burton, N. P.; O'Hagan, N. High-throughput assays for DNA gyrase and other topoisomerases. *Nucleic Acids Res.* **2006**, *34*, e104.
(51) Quattropani, A.; Rueckle, T.; Schwarz, M.; Dorbais, J.; Sauer, W.; Cleva, C.; Desforges, G. Thiazole Derivatives and use Thereof. PCT Int. Appl. WO 2005068444, Jan 12, 2004.
(52) *OMEGA 2.4.6*; OpenEye Scientific Software, Inc.: Santa Fe, NM, 2012.
(53) *Protein*; National Center for Biotechnology Information, U.S. National Library of Medicin: Bethesda, MD; http://www.ncbi.nlm.nih.gov/protein (Accessed May 21, 2012).
(54) Sievers, F.; Wilm, A.; Dineen, D.; Gibson, T. J.; Karplus, K.; Li, W.; Lopez, R.; McWilliam, H.; Remmert, M.; Soding, J.; Thompson, J. D.; Higgins, D. G. Fast, scalable generation of high-quality protein multiple sequence alignments using Clustal Omega. *Mol. Syst. Biol.* **2011**, *7*, 539.
(55) Niesen, F. H.; Berglund, H.; Vedadi, M. The use of differential scanning fluorimetry to detect ligand interactions that promote protein stability. *Nature Protoc.* **2007**, *2*, 2212−2221.
(56) de Mol, N. J.; Fischer, M. J. E. Surface plasmon resonance: a general introduction. *Methods Mol. Biol.* **2010**, *627*, 1−14.
(57) Rich, R. L.; Myszka, D. G. Grading the commercial optical biosensor literature-Class of 2008: "The Mighty Binders". *J. Mol. Recognit.* **2010**, *23*, 1−64.
(58) Kampranis, S. C.; Gormley, N. A.; Tranter, R.; Orphanides, G.; Maxwell, A. Probing the binding of coumarins and cyclothialidines to DNA gyrase. *Biochemistry* **1999**, *38*, 1967−1976.
(59) Jerabek-Willemsen, M.; Wienken, C. J.; Braun, D.; Baaske, P.; Duhr, S. Molecular interaction studies using microscale thermophoresis. *Assay Drug Dev. Technol.* **2011**, *9*, 342−353.
(60) Saiz-Urra, L.; Cabrera, M. A.; Froeyen, M. Exploring the conformational changes of the ATP binding site of gyrase B from *Escherichia coli* complexed with different established inhibitors by using molecular dynamics simulation: protein−ligand interactions in the light of the alanine scanning and free energy decomposition methods. *J. Mol. Graphics Modell.* **2011**, *29*, 726−739.
(61) Otwinowski, Z.; Minor, W. Processing of X-ray Diffraction Data Collected in Oscillation Mode. *Methods Enzymol.* **1997**, *276*, 307−326.
(62) McCoy, A. J.; Grosse-Kunstleve, R. W.; Adams, P. D.; Winn, M. D.; Storoni, L. C.; Read, R. J. Phaser crystallographic software. *J. Appl. Crystallogr.* **2007**, *40*, 658−674.
(63) Murshudov, G. N.; Vagin, A. A.; Dodson, E. J. Refinement of macromolecular structures by the maximum-likelihood method. *Acta Crystallogr., Sect. D: Biol. Crystallogr.* **1997**, *53*, 240−255.
(64) Turk, D. Weiterentwicklung eines Programms fuer Molekuelgraphik und Elektrondichte-Manipulation and Seine Anwendung auf Verschiedene Protein-Strukturaufklerungen. Ph.D. Thesis. Technische Universitaet Muenchen, Muenchen, Germany, 1992.
(65) Andrejasic, M.; Prašnikar, J.; Turk, D. PURY: a database of geometric restraints of hetero compounds for refinement in complexes with macromolecular structures. *Acta Crystallogr., Sect. D: Biol. Crystallogr.* **2008**, *64*, 1093−1109.